Optical vector vortices generated with circularly planar and circularly hybrid nematic cells

[1] Dudok T., [1] Skab I., [1] Mys O., [2] Krupych O., [3] Nastishin Yu. A., [4] Kurochkin O., [4] Nazarenko V., [3] Ryzhov Ye., [3] Chernenko A. D. and [1] Vlokh R.

[1] O. G. Vlokh Institute of Physical Optics, 23 Dragomanov Street, 79005 Lviv, Ukraine
[2] Ivan Franko National University of Lviv, Faculty of Electronics and Computer Technologies, Department of Optoelectronics and Information Technologies, 107 Tarnavskyi Street, 79017 Lviv, Ukraine
[3] Hetman Petro Sahaidachnyi National Army Academy, 32 Heroes of Maidan Street, 79012 Lviv, Ukraine
[4] Institute of Physics, National Academy of Sciences of Ukraine, Kyiv 03028, Ukraine

Received: 30.11.2022

Abstract. Among the variety of optical elements used for the generation of vector and vortex light beams, liquid-crystal cells containing topological defects deserve a special attention. Nowadays, they represent one of the most popular techniques because of simplicity of their preparation. In this work we study optical singularities of the laser beams passing through a cell with a circular planar alignment of its director on both substrates, a so-called CC-cell. The other subject is a CH-cell with a circular planar alignment on one substrate and a homeotropic (i.e., perpendicular to the substrate plane) alignment on the opposite substrate. The CC- and CH-cells are characterized optically with both polarization optical microscopy and imaging polarimetry. The optical singularities of the object beams passing through these cells are visualized by means of their interference with quasi-spherical and quasi-plane-wave reference Gaussian beams. For the CC-cells, one expects formation of the defects with the topological strength $q = +1$ on the surfaces. Due to an effect of escape into a third dimension, a singular director distribution does not propagate through the bulk. While reviewing the literature on the applications of liquid-crystal disclinations for generating the singular beams, we have found that the escape of the director into the third dimension is usually ignored for integer-strength disclinations. We also analyze in detail how the escape into the third dimension manifests itself when the light propagates through the CC-cells. For the case of CH-cells, we find that the optical patterns obtained with the polarization optical microscopy, the imaging polarimetry and the interference techniques indicate that the circular symmetry of a sample structure is essentially broken.

Keywords: liquid crystals, optical vortices, topological defects, optical indicatrix, optical phase difference

UDC: 535.34, 535.37, 544.25

1. Introduction

Light is one of the most intensely and long studied states of matter which, nonetheless, still remains a mystery. The mystery of the light and its vital importance for all living creatures are hard to overestimate. Although the light is with us everywhere, being the most accessible to study, it does not cease to amaze. Impressive is not only the depth of our knowledge; the depth of our

nescience about it is even more striking and permanently shown up by new and new discoveries and applications. From our earliest moments, we experience this state of matter as something soft, fluid, seemingly disordered, apparently like a liquid. Multiple analogies with a liquid state are fruitful from naive or poetic epithets in our everyday life to scientifically justified theoretical analogies in electromagnetism, which is the essence of the light as a state of matter. By the way, being disordered internally, a liquid can be structured externally: amazingly beautiful thermo-capillary Marangoni patterns come to mind in this respect [1]. It turns out that the light can also be structured, with not less beautiful patterns driven by different underlying mechanisms.

A structured light [2] is a modern trend in optics, which deals with light patterning. Being a field of intense researches, the structured light finds applications in many novel branches of optical technologies such as 3D scanning [3], 3D photographing of fingerprints [4], etc. The light can be structured by its amplitude, phase and polarization. Singular laser beams structured by their phase and amplitude (scalar-field singularities) or by the amplitude, phase and polarization (vector-field singularities) are among the recent advances in optics. They are termed respectively as scalar-vortex (most frequently called simply as 'vortex') [5] and vector-vortex beams [6]. These structured beams bear mathematical singularities in the fields of their optical parameters. They have already found multiple applications in such newly arisen areas as quantum communications and information technologies [7, 8], sharp focusing [9, 10], optical trapping [11], phase mask coronagraphy [12] and particle acceleration [13, 14].

The methods for generation of the singular beams have been developing rapidly in the last two decades. The first (and, in fact, the most popular) method, which has already become classic, is a method of computer-synthesized holograms [15] for generating the scalar optical vortices. It is quite simple in its realization since the grating with a fork-like bifurcation can be fabricated with a usual printer. However, the original version of this method has principal limitations concerned with the possibilities of operation by the positions of vortices and their parameters. Spatial light modulators which form desired phase and amplitude distributions by holographic recording [16] overcome this inconvenience. Electrically and optically addressed liquid-crystal (LC) spatial light modulators are more handy and free of most of the inconveniences inherent to their counterparts. The possibility of simultaneous generation of multiple vortices on the same screen is their undeniable advantage [17]. So-called spiral phase plates fabricated via coating [18] bear the same inconvenience of a stationary inoperable pattern, which is typical for the computer-synthesized holograms. Moreover, production of the spiral phase plates for the optical wavelengths requires complicated and highly precise technologies. The computer-synthesized holograms and the spiral phase plates are usually designed for the generation of scalar-field singularities.

Several methods have been developed for the generation of vector-field singularities. They employ LCs [19, 20], solid single crystals under mechanical torsion and bending and in a conically distributed electric field [21–23], space-variant sub-wavelength gratings [12, 24–26], intracavity merging of laser modes [27], and interferometry [28]. The optical elements generating the vector vortices are also classified by their function. So-called *J*-plates [29] are designed for coupling the spin and orbital angular momentums of light, where *J* refers to the total angular momentum of a photon. In this paper, we will deal with a so-called *q*-plate, which represents the optical device for generating a light beam with a nonzero orbital angular momentum out of a beam with a well-defined spin angular momentum.

A traditional design of the *q*-plates is based on a propagation of polarized light through an LC disclination [30–32]. At least two different approaches are available for shaping the LC

disclinations. First, one can employ polarization-optical textures with various defects in LC samples. They are formed spontaneously due to certain geometric or surface-anchoring conditions such as those appearing in the freely suspended LC droplets, in the LC films freely suspended or deposited on an isotropic liquid or in the LC cells with untreated substrates [33, 34]. In particular, manipulation of the orbital angular momentum of light at the micron scales with the nematic disclinations of different topological strengths $q = l/2$ (with the integer l values lying in the interval $-3 < l < 3$) in the nematic doped with a non-mesogenic material has been demonstrated in Ref. [35]. It is worth noting that, by its value, the orbital angular momentum l commonly accepted in the terminology on singular light beams coincides with the Frank index $l = 2q$ [36] of the corresponding topological defect.

The second approach for producing the LC disclinations can be implemented by either configuring a desired singular distribution of the nematic director in an LC-based spatial light modulator or aligning in a special manner the nematic director in manually prepared LC cells. The generation of integer and fractional vector beams with the *q*-plates encoded onto spatial light modulators has already been reported [37]. Programmable optical-vortex lattices generated in an LC valve with the spatial light modulator has been employed [38] to convert an array of circularly polarized input beams into an output array of vortex beams with the topological charges governed by LC defects. A so-called meta-*q*-plate with arbitrarily space-variant optical axes, which has been fabricated in the work [39] via the LC photo-alignment based on a polarization-sensitive alignment agent and a dynamic micro-lithography system, demonstrates enhanced capabilities for vortex-beam shaping. In Ref. [40], the disclination has been generated in a nematic LC cell doped with an azo-dye, using the photo-alignment technique in the geometry where both the cell and the linear polarizer are rotated.

An attractive, remarkably simple and cheap technique for fabricating the *q*-plates has been offered by the author [41] It does not require sophisticated techniques like photo-lithography or polymer photo-alignment which might not be accessible in each laboratory. Instead, the method can be employed by a user having beginner skills in the fabrication of aligned LC cells. According to the approach [41], the *q*-plate represents a nematic LC cell assembled of two substrates, one of which is circularly rubbed with a velvet clothing and the other one is either a cleaned bare or polyimide-coated glass. Such an untreated substrate is expected to produce an azimuthally degenerate planar alignment for nematic molecules. The results [41] demonstrate that the *q*-plate of this kind is indeed efficient for generating the optical beam with a helical wavefront and a singularity with the topological strength $q = l/2$ ($l = \pm 2$). The idea of such a cell geometry is that the circular rubbing can form the defect with the topological strength $q = +1$ in the nematic-director field at the substrate, while "the other glass was left un-rubbed, for degenerate planar alignment" [41]. The idea associated with the azimuthally degenerate planar alignment is that, under the condition of azimuthally degenerate planar anchoring, the nematic molecules would be free to align along any azimuthal direction at no energy cost, in order to avoid additional director-field deformations and defects which might appear due to competition between the directions of easy axes taking place at the opposite bounding substrates. However, the fact that the substrate has not been rubbed does not ensures the *degenerate* planar anchoring conditions. The experiments [42, 43, 44] suggest that most solid substrates exhibit a property of surface memory. Due to this effect, the distribution of the nematic director is spatially fixed within the substrate plane, thus implying a nonzero azimuthal anchoring for the realignment, even though the azimuthal director orientation might be random.

In addition to the surface-memory effect, most solid substrates provide a nonzero pre-tilt angle of the director (in the zenithal plane) with respect to the substrate surface. Both azimuthally degenerate anchoring and random anchoring with a nonzero pre-tilt of the director might lead to the formation of additional defects near the un-rubbed substrates, often forming a known Schlieren texture. We argue that the surface-memory property and the nonzero director pre-tilt might bring uncontrolled distortions in the director-field distribution at the un-rubbed substrates. To avoid the competitive orientations of the director at the opposite substrates, the authors [41] heat the cell to the isotropic phase and then slowly cool it down while keeping the temperature gradient along the cell normal. In this way the nematic phase nucleated at the rubbed substrate can slowly extend to the opposite substrate. Although one can prepare by chance a cell seemingly with no undesirable distortions, the quality and reproducibility of the alignment at the un-rubbed substrate seem to be rather poorly controllable. Indeed, it is stated in Ref. [41] that the un-rubbed polyimide-covered substrate and the bare-glass substrate require different rubbing pressures and durations to get a satisfactory alignment. In the present work, we test the two possibilities in order to avoid uncontrollable alignments occurring at the un-rubbed substrate. For this aim, we first prepare a cell with both substrates being circularly rubbed (a CC-cell). Second, we replace the un-rubbed substrate by the substrate providing a homeotropic (i.e., perpendicular to the substrate) alignment for the uniaxial nematic director, which is azimuthally degenerate (a CH-cell).

Another problem which we raise in this study concerns a topological stability of the nematic-wedge disclinations which are used for generating the singular beams. Namely, semi-integer- and integer-strength disclinations belong to different topological classes. The core of the integer-strength disclination can be smoothly transformed into a non-singular director configuration, while the core of the disclination with the semi-integer strength is always singular. The mechanism of transformation of the integer-strength disclinations into non-singular configurations is often called ‘an escape of the director into a third dimension’. This effect has been predicted theoretically and confirmed experimentally by M. Kleman and P. Cladis [45]. Somewhat later, this effect has been found independently by R. Meyer [46] for the case of integer-strength disclinations in a capillary with the homeotropic director alignment taking place at the capillary surface. D. Melzer and F. R. N. Nabarro [47] have demonstrated that the integer-strength disclinations also manifest the escape of the director into a third dimension in the capillaries with the circularly planar director alignment. When reviewing the literature on the generation of the singular beams with the LC disclinations, we have revealed that the escape into the third dimension is usually ignored for the integer-strength disclinations. The cells used in the literature for generating the singular beams are relatively thin (typically 5–6 μm), so that they produce the optical phase retardation $\lambda/2$ to achieve the full spin-to-orbit angular-momentum conversion [48]. To examine the effect of the escape into the third dimension on the structure of the singular vector beams, we will deal with much thicker cells (~ 20 μm). Using an imaging polarimetry technique, we will also demonstrate unambiguously that the effect of the escape mentioned above does manifest itself for the circular disclinations with the topological strength $q = +1$.

The paper is organized as follows. The experimental details of cell preparation are given in Section 2. Our preliminary theoretical considerations show that optics of the vector beams gets much richer for light-absorbing fluorescent media. For this reason we have doped nematic under study with a fluorescent dye. Several effects can be expected due to a light absorption. In particular, the fluorescence and the laser generation in dye-doped LCs [49–55] open a possibility for generating the optical singularities in the fluorescent or laser light. Although in this paper we

do not deal directly with the light absorption, the fluorescence and the laser generation (they will be the subjects of our forthcoming studies), in Section 3 we characterize optically the dye-doped cells with a circularly planar (on both substrates) director alignment and a hybrid (i.e., circularly planar on one substrate and homeotropic on the other) director alignment, using the imaging polarimetry. Moreover, we examine the structure of the singular object beams emergent from the cells by means of their interference with the reference beams having quasi-spherical and quasi-plane Gaussian wavefronts. Finally, Section 4 summarizes the main conclusions drawn in the present study.

2. Fabrication of nematic cells and experimental procedures

The cells were assembled of two glass substrates which were spin-coated with polymer alignment layers. The substrate for the planar alignment was covered by Kapton polyimide and circularly rubbed with a velvet clothing using a motor. To get the homeotropic alignment, a substrate was spin-coated with an SE-1211 polymer (Nissan Chemicals). Both substrates of the CC-cell were circularly rubbed in the same direction and then faced by their polymer surfaces such that the two polymer-covered surfaces were turned inwards with respect to the cell. In this manner, the rubbing directions on the opposite substrates were anti-parallel. We note that assembling of the cell with the anti-parallel rubbings on the opposite substrates provides the same signs of the director pre-tilts on both substrates. In case of the parallel rubbing, the zenithal tilts of the director at the opposite substrates would be mirror-symmetric with respect to the cell mid-plane. For both the CC- and CH-cells, the substrates were fixed together, using a photo-sensitive glue dotted along the two opposite sides on one of the substrates. Cylindrical spacers with the thickness 20 μm were dispersed in glue to provide a uniform thickness of the cell gap. The cell was filled with E3100-100 nematic (Merck). It was doped with 0.8 wt. % of a Nile Red dye after the cell had been heated up to the temperature 10°C above the nematic-clearing point. The linear birefringence of nematic measured in our laboratory was equal to $\Delta n = 0.1493$ at the light wavelength $\lambda = 632.8$ nm .

Polarization textures of the cells placed between crossed linear polarizers were recorded with a CCD camera by illuminating the cells with a He-Ne laser under polarization optical microscope (Fig. 1a) and on an optical holographic table (Fig. 1b). The main difference of the two observation geometries is in the diameter of view field, which is ~ 5 mm for the microscope and ~ 16 mm for the image detected with the CCD camera on the optical bench. In both observation geometries, the light propagates perpendicular to the cell substrates. It is optically collimated to minimize the beam divergence.

To build spatial maps of the orientation of optical indicatrix and the optical phase difference, we used an imaging polarimetric setup (the laser wavelength $\lambda = 632.8$ nm) described earlier in Ref. [21]. While measuring the phase difference, we utilized a circularly polarized probing laser beam, thus making the output signal insensitive to the azimuthal orientation of the optical indicatrix. In the framework of a linear phase-retarder model and for a given azimuthal angle α of analyzer, the output intensity I reads as

$$I(\alpha) = \frac{I_0}{2}\left\{1 + \sin\Delta\Gamma \sin\left[2(\alpha - \theta)\right]\right\} = C_1 + C_2 \sin\left[2(\alpha - C_3)\right], \quad (1)$$

where $\Delta\Gamma$ is the phase retardation, θ the azimuthal orientation of the eigenvectors of the optical indicatrix, and C_i the constants. By fitting the dependence $I(\alpha)$ measured for each pixel of the digital image, one can find the fitting coefficients

$$C_1 = \frac{I_0}{2},\ C_2 = \frac{I_0}{2}\sin\Delta\Gamma,\ C_3 = \theta, \tag{2}$$

from which the phase retardation $\Delta\Gamma$ is calculated as

$$\sin\Delta\Gamma = C_2 / C_1. \tag{3}$$

Then the azimuth of the analyzer corresponding to the intensity minimum would give the azimuthal orientation θ which is equal to the fitting coefficient C_3. Using the fitting results, one can plot 2D maps of the optical phase difference and the optical-indicatrix orientation.

To visualize the optical singularities of light beams, we studied the interference patterns using a Mach–Zehnder interferometer. A sample under test was inserted into one of the arms of this interferometer. The circular polarizers were crossed to achieve a pure vortex mode. A light beam with either quasi-plane or quasi-spherical wavefronts propagated in the other interferometer arm. For simplicity, further on we will omit the words 'Gaussian' and 'quasi-' in such long though rigorous terms as 'the Gaussian beam with the quasi-spherical (or quasi-plane) wavefront'. The spherical wavefront was formed using a lens with the focal length 1 m. Finally, a doughnut-mode patterns for the singular beams were detected on the CCD camera with the cells placed between the crossed circular polarizers.

3. Results and discussion

3.1. Polarization textures

The CC-cell manifests the polarization textures with four mutually perpendicular extinction brushes. We have a Maltese cross when viewing in a white light between the crossed polarizers under the microscope (Fig. 1a) and in a gray-scale mode with the CCD camera on the optical holographic table (Fig. 1b). This occurs for the laser illumination with either $\lambda = 632.8$ nm or $\lambda = 532$ nm. The axes of the extinction brushes are along the transmission directions of the polarizer and analyzer, which is expected for the planar circular director distribution.

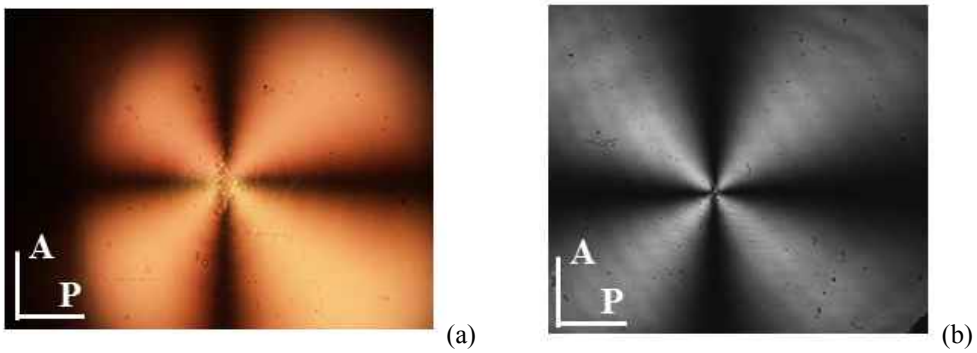

(a) (b)

Fig. 1. Polarization textures of the CC-cell as viewed (a) under polarization microscope in white light and (b) with CCD camera in a gray-scale mode under laser illumination (λ = 632.8 nm).

The polarization-microscopy texture for the CH-cell also involves the Maltese cross, although the axes of the corresponding extinction brushes (shown by dashed lines in Fig. 2) appear to be rotated by about 6^o with respect to the transmission directions of the crossed polarizers (shown by solid lines in Fig. 2). The directions of rotation of the brushes are opposite for the face-up and face-down settings of the CH-cell. Namely, we have clockwise and anti-clockwise directions for the face-up and face-down settings. In the face-up setting (denoted for convenience as CH), the light meets first the C-substrate with the circular surface director alignment. In the

face-down setting (denoted as HC), the cell is rotated around the in-plane axis such that the light enters the cell from the side of the homeotropic H-substrate. The azimuthal orientation of the cell in Fig. 2a is the same for both the CH- and HC-settings. When the microscope stage rotates azimuthally, the extinction brushes apparently remain mutually perpendicular and preserve the same orientation, 6°, with respect to the crossed polarizers.

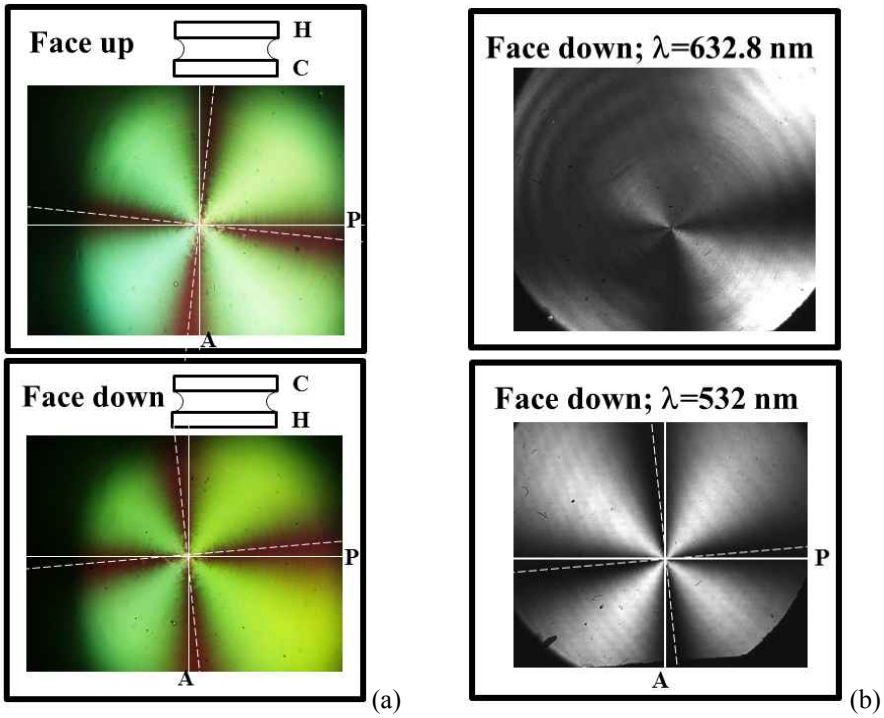

Fig. 2. Textures of the CH-cell as observed (a) under polarization microscope in white light and (b) on holographic table under laser illumination. The axes of the extinction brushes (shown by dashed lines) are rotated by 6° with respect to the transmission directions of polarizers (shown by solid lines). The rotation direction is clockwise in case of the face-up (CH) setting and counter-clockwise in case of the face-down (HC) setting.

Similarly, the Maltese cross rotated by the same angle (about 6°) is observed with the CCD camera (in the gray-scale mode) when the cell is illuminated with the green (λ = 532 nm) laser on the optical holographic table (see the bottom photograph in Fig. 2b). Under the illumination with the red (λ = 632.8 nm) laser, only two of four extinction brushes are clearly visible, while the others are characterized by a low contrast (see the top photograph in Fig. 2b). Such a pattern might be an evidence that the azimuthal director distribution is not circularly symmetric. Brightening of the extinction brushes suggests that the director is significantly twisted around the axis parallel to the cell normal. Consequently, this leads to polarization rotation of light propagating through the twisted structure. Therefore, the darkest extinction brush is located in the place where the in-plane projection of the director is roughly parallel to the transmission direction of the polarizer (or the analyzer) and the twist through the cell thickness is minimal (close to 0°). On the contrary, the brightest brush visualizes the place where the light polarization rotation is close to 90°, which in turn implies a significant director twist. Most probably, the director rotates through the cell thickness along helical lines. Note that the optics of gyrotropic absorbing media is a complicated matter [56–60] which deserves a special consideration. This will be a subject of our forthcoming work.

Although the polarization-microscopy texture of the CH-cell observed in the white light (Fig. 2a) shows four well-defined extinction brushes, it also contains the features signalling that the structure is not symmetric around its centre. Namely, the interference colours between the extinction brushes are not circularly uniform. The background is greenish in the second quadrant and yellowish in the fourth quadrant. Different interference colours indicate a difference in the optical phase retardations. In its turn, this reveals the difference in the structures of the director field.

The difference between the patterns of Fig. 2a and Fig. 2b observed for the CH-cell can be attributed to different spectra of illuminating light. The texture is observed in the white light under the polarization microscope (Fig. 2a), whereas the sample placed on the optical holographic table is illuminated with either red (λ = 632.8 nm) or green (λ = 532 nm) monochromatic laser light (see respectively the bottom and top photographs in Fig. 2b). Therefore, we are led to conclude that the rotation of light polarization due to the director twist is highly dependent on the light wavelength, such that the rotation for the red light is larger than that for the light of shorter (yellow or green) wavelengths. It should be noted that the intensity of the microscope lamp is usually maximal in the green-yellow part of the spectrum around λ = 530 nm. It is just this part of the spectrum that governs the appearance of the polarization-microscopy texture. If the polarization rotation in this spectral region (around λ = 530 nm) is weak, then it is natural that all the four extinction brushes are clearly visible in the green laser light (λ = 532 nm – see the pattern in Fig. 2b).

It is also worth noting that the spectral region around λ = 530 nm, in which one observes the four well-defined extinction brushes under the microscope, corresponds to the maximum of the absorption band detected for our dye-doped nematic [33]. It is likely that brightening of the extinction brushes due to light polarization rotation by the twisted structure of the director is accompanied by their darkening due to light absorption by the dye molecules which are parallel to the principal directions of the polarizer or analyzer. The light absorption of our material in the red light (λ = 632.8 nm) is negligible [33], whereas the gyrotropy might be high enough. The hybrid alignment together with the twist of the nematic director lower the symmetry of the sample, which should in fact be considered as an optically biaxial medium. The eigenwaves propagating in a biaxial absorbing gyrotropic medium might have a nonzero ellipticity. Our preliminary considerations show that the ellipticity of the eigenwaves might indeed brighten the extinction brushes observed in the crossed polarizers. We do not explore these considerations further on, leaving it for the future work.

The spectral dependence of the light polarization rotation could be expected if the light propagation through a twisted nematic cell is close to the limit of the Mauguin regime [61]. The condition

$$\left(\pi/\Delta\theta\right) d\Delta n_{eff} \gg \lambda \tag{4}$$

corresponds to the Mauguin regime, at which the light polarization follows the rotation of the nematic director in the cell. Here d denotes the cell thickness, $\Delta\theta$ the difference between the azimuthal angles of the director at the two opposite cell substrates, and $\Delta n_{eff} = \Delta n \sin^2\beta$ is the effective birefringence of the nematic the director of which is tilted with respect to the cell normal by the zenithal angle β. Under the condition opposite to that given by Eq. (4), the light polarization rotation is significantly retarded if compared with the director rotation. Thus, the polarization rotation tends to become smaller when the limit of the Mauguin regime is approached and below this limit.

For the hybrid-aligned cell, the zenithal angle β of the director changes from 90° at the planar substrate to 0° at the homeotropic one. Were the director planar through the overall cell thickness, the effective birefringence Δn_{eff} would be equal to its maximal value, which is $\Delta n = 0.149$ for our nematic. Then the condition (4) would be surely satisfied for such a large pitch p of the twist, which is of the order of $4d = 80$ μm for the twisted nematic cell. However, the director in the hybrid CH-cell is significantly tilted with respect to the cell normal, which implies that Δn_{eff} is significantly smaller than Δn. For a linear dependence $\beta(z)$ of the zenithal angle β on the coordinate z along the cell normal, the estimation gives $\Delta n_{eff} = (\Delta n/d)\int_0^d \sin^2\left(\frac{\pi}{2}\frac{z}{d}\right) = \frac{\Delta n}{2}$. Then the maximal possible azimuthal rotation of the director could be $\Delta\theta_{\max} = \pi/2$, which corresponds to the pitch $p = 4d$ of the twist. For $d = 20$ μm and $\Delta n = 0.15$, we find $(\pi/\Delta\theta_{\max})d\Delta n_{eff} = 3$ μm, which is considerably larger that the light wavelength $\lambda = 0.6328$ μm. Hence, the Mauguin condition (4) must hold true. The pitch for the smaller values $0 < \Delta\theta < \pi/2$ would be even longer, $p > 4d$. Then the parameter $(\pi/\Delta\theta_{\max})d\Delta n_{eff}$ would be even larger and, hence, the Mauguin condition (4) would hold even better. Therefore shortening of the light wavelength from red to green should not lead to decrease in the light polarization rotation in any twisted-director structure. Therefore, the escape from the Mauguin regime can be ruled out in the green-yellow spectral region.

3.2. Imaging polarimetry

3.2.1. The CC-cell. To study the polarization structure of the beams emerging from the LC cells, we plot the maps of the light polarization-ellipse orientation and the phase retardation in our LC cells, which have been measured with the imaging polarimeter. Fig. 3a shows that the azimuth of the light-polarization ellipse for the CC-cell is circularly distributed around the core of the nematic defect. This qualitative conclusion is confirmed by the quantitative data, i.e. the linear dependence of the azimuth θ of the polarization ellipse on the azimuthal angle φ (see Fig. 3c). Expectedly, the full φ rotation by 360° corresponds to the θ rotation by 360°. Therefore, the absolute value of the topological strength of the nematic defect in the CC-cell is equal to $|q| = 1$. This agrees with the circular director distribution which is set by the circularly rubbed substrates. Fig. 3a reveals that φ and θ are of the same sign. In other words, the polarization ellipse of the emergent beam rotates in the direction which coincides with the direction of navigation along a closed circuit around the defect core. In its turn, this fact indicates that the sign of the strength of the nematic defect is positive, i.e. we have $q = +1$. Such a topological defect is expected to generate an isotropic optical vortex [62].

Fig. 3b and Fig. 3d show that the optical phase retardation Γ gradually drops from the periphery of the defect (the radial coordinate $\rho \sim 1$ mm), where it is $\Gamma|_{\rho\sim 1mm} \approx 180° \times m + 80°$, down to the value $\Gamma|_{\rho\sim 0mm} \approx 180° \times m + 5°$ at the defect centre ($\rho \sim 0$ mm). Note that our polarimetric technique measures the phase retardation up to the factor πm, where m is an

integer. For the birefringence $\Delta n = 0.1493$ and the cell thickness $d = 20$ μm, one can find the maximal possible optical phase retardation $\Gamma = 2\pi \frac{\Delta n d}{\lambda} \approx 9 \times 180° + 78° = m\pi + \Delta\Gamma$, which corresponds to the planar director orientation through the cell thickness. Assuming that the director orientation remains planar through the cell thickness far from the defect centre, we find $m = 9$ and estimate the excessive phase retardation as $\Delta\Gamma = 78°$. It is quite close to the corresponding value $\Delta\Gamma\big|_{\rho \sim 1\,\text{mm}} \approx 80°$ measured experimentally at the defect periphery, i.e. at the radial coordinate $\rho \sim 1$ mm. Since the variation of the measured excessive retardation $\Delta\Gamma(\rho)$ as a function of the radial coordinate ρ towards the defect centre is monotonic, one can conclude that the full phase retardation $\Gamma(\rho)$ changes from $\Gamma\big|_{\rho \sim 1\,\text{mm}} \approx 9 \times 180° + 78°$ at the periphery of the defect to $\Gamma\big|_{\rho \sim 1\,\text{mm}} \approx 9\pi$ in the vicinity of the nematic disclination core. In an ideal case corresponding to the model of isotropic disclination core, one would expect that the phase retardation drops to zero inside the disclination core. The same is expected for the defect core in terms of the optical singularity. The real situation is somewhat different. Fig. 1a and Fig. 2a show that the disclination core is essentially imperfect at the centre. Nonetheless, the optical technique detects the optical singularity in the centre of the patterns shown in panels a, b and d of Fig. 3.

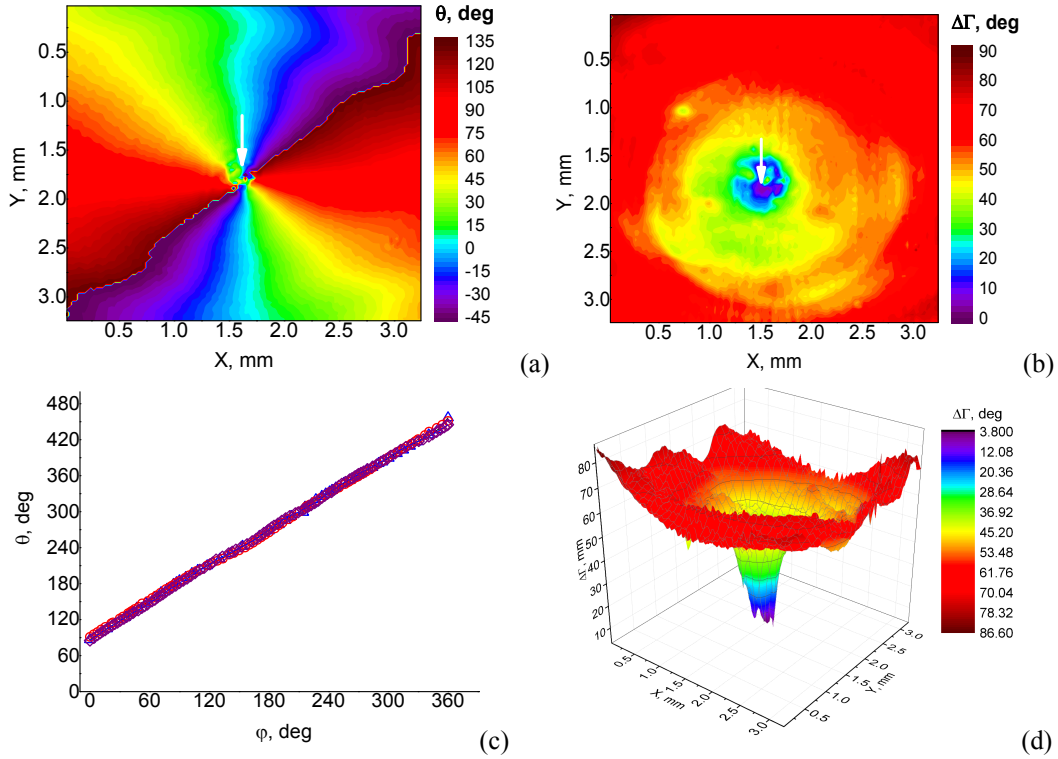

Fig. 3. Maps of the orientations of eigenvectors of optical indicatrix (a) and optical phase difference (b), dependence of the optical-indicatrix orientation angle on azimuthal angle (c) at ρ = 0.46 mm (open triangles), 0.81 mm (open circles) and 1.22 mm (open diamonds), and dependence of the phase difference on the *X* and *Y* coordinates (d) in the CC-cell. The location of defect is indicated by a white arrow.

A gradual decrease in the excessive phase retardation $\Delta\Gamma(\rho)$ along the radial coordinate suggests that the director is not parallel to the substrates in the bulk of the cell. Rather it tends to escape from this plane when the axis of the structure is approached, in order to avoid the singularity in the bulk when distancing from the substrates. This effect is known in the LCs as an 'escape of the director into a third dimension' [45, 47, 63, 64]. Topological and elastic energy considerations suggest that the core of the integer-strength disclination is unstable against the escape into a third dimension. For the ideally planar circular director distribution, which is singular at the centre, the director field would have the form

$$\vec{n}(x;y;z)=\left[n_x=\cos\theta;\, n_y=\sin\theta;\;\; n_z=0\right], \tag{5}$$

while for the director configuration escaped into the third dimension we obtain

$$\vec{n}(x;y;z)=\left[n_x=\cos\theta\sin\beta(\rho;z);\, n_y=\sin\theta\sin\beta(\rho;z);\;\; n_z=\cos\beta(\rho;z)\right]. \tag{6}$$

Here $\beta(\rho;z)$ is the zenithal angle of the director measured with respect to the cell normal at the distance z from the substrate. For the director configuration which is circularly symmetric with respect to the axis aligned with the cell normal, one has $\theta=\varphi$, where φ is the zenithal angular coordinate of the cylindrical coordinate system $(\rho;\varphi;z)$ (with z amounting to $z=0$ on the lower cell substrate and $z=d$ on the upper one). One of the possibilities for the director to escape into the third dimension is a configuration of a 'double-twist cylinder'. If the axis of the double-twist cylinder is along the cell normal, the director on the double-twist cylinder axis would be parallel to the cylinder axis and rotate around its radius from $\beta\big|_{\rho=0}=0$ on the axis to $\beta\big|_{\rho=R}=\pi/2$ at the periphery of the cylinder. For the double-twist cylinder uniform along the z coordinate, the β parameter would read as

$$\beta(\rho,z)=\frac{\pi}{2}\frac{\rho}{R}, \tag{7}$$

where R is the radius of the double-twist cylinder. The non-escaped and escaped configurations have different elastic energies. The non-escaped configuration involves only bending deformations, while the bending deformation in the escaped configuration is partially replaced by the twist deformation. Taking into account that the twist elastic constant K_2 for most of conventional low-molecular thermotropic nematics is smaller than the bend constant K_3, one concludes that the escaped configuration has a lower bulk elastic energy. In addition, the escaped configuration is not singular, which implies an additional gain in the elastic energy if compared with the non-escaped configuration.

However, the escaped configuration implies some energy cost to overcome the surface anchoring at the substrate. Typically, the surface anchoring is quite strong for a rubbed-polymer substrate. To prove this, one can compare the appropriate value $\geq 10^{-3}$ J/m^2 with $\sim 10^{-6}$ J/m^2 typical for the homeotropic anchoring [65–67]. For the infinitely strong zenithal anchoring, the director remains parallel to the substrate surface near the substrate and escapes into the third dimension inside the bulk. Therefore, the zenithal angle $\beta(\rho;z)$ should be a sigmoid function [68, 69] of the z coordinate, such that we have $\left|\beta(\rho;z=0)\right|=\left|\beta(\rho;z=d)\right|=\pi/2$. The β value is

given by Eq. (7) inside the mid-plane of the cell (i.e., at $z = d/2$). Then $\beta(\rho;z)$ can be modelled by the function

$$\beta(\rho,z) = \frac{\pi}{2} - 2\frac{R-\rho}{R}\left[\frac{\pi}{4} - \sqrt{\left(\arctan\left(1-2\frac{z}{d}\right)\right)^2}\right]. \tag{8}$$

In the case of infinitely strong anchoring, one expects that the escape into the third dimension represents a threshold effect. Namely, it would take place only if the thickness d of the cell is larger than the threshold thickness d_{th}. For this reason we use rather thick 20-μm cells.

Let us note that the double-twist cylinder is a chiral structure which can be either left- or right-handed. The nematic studied by us is not chiral. Thus, both the left- and right-handed twists are equally probable. Then one should expect that the double-twist cylinder is split into two domains of opposite chiralities. However, it should be taken into account that the circular rubbing of the substrate is also either left- or right-handed. Were the pre-tilt angle of the director at the substrate exactly zero, the chirality sign of the circular rubbing would not show up in the director structure. Otherwise, the circular rubbing with a nonzero director pre-tilt at the substrate surface breaks the chiral symmetry and the twisted structure adapts the chirality sign of the circular rubbing.

Finally, the optical phase retardation (in radian units) of the cell can be calculated as

$$\Gamma(\rho;z) = \frac{2\pi}{\lambda}\int_0^d \Delta n \sin^2\beta(\rho;z)dz, \tag{9}$$

with β given by Eq. (8). The model suggested above accounts for the radial dependence of the optical phase retardation which is maximal at the periphery of the structure and drops down gradually when its centre is approached. Let us recall that this model is based on the assumption that the director configuration remains circularly symmetric even after the director escapes into the third dimension. However, it is seen from Fig. 2b that the map of the optical phase retardation is considerably imperfect. One of the possibilities is that these imperfections are related to imperfections of the circular rubbing, including those located nearby the centre. An alternative possibility is that a break of the circular symmetry is a spontaneous effect, which lowers the elastic energy in a way similar to that reported in Refs. [70, 71] for the hybrid-aligned nematic films. This occurs via insertion of the sectors where the director configuration has an essentially non-circular symmetry. The nature of these imperfections still needs to be elucidated.

Anyhow, the experimental data shown in Fig. 3b demonstrate unambiguously that, even in a cell assembled of the two circularly rubbed substrates (i.e., in the CC-cell), the director configuration appears to be more complicated than one could expect. First, due to the escape into the third dimension, the director-field lines do not form concentric cylinders and, second, the circular symmetry seems to be broken. Importantly, the escape of the director into the third dimension is not a configuration which is specific solely to the cells studied in this paper. It should be a rather common situation in the nematic cells with a circularly symmetric director alignment at the surface. We expect that the *q*-plates based on the nematic cells with the circular director distribution reported earlier [41] should also reveal the escape into the third dimension. It is important that the escape of the director into the third dimension can take place in the q-plates with the integer value $q = 1$ rather than the semi-integer value $q = 1/2$. This is a topological restriction.

The disclinations with semi-integer and integer strengths belong to different topological classes of defects: the core of a semi-integer-strength disclination is mandatorily singular and that of an integer-strength disclination is not [72, 73]. The escape of the director into the third dimension is a mechanism for topologically continuous transformation of a singular core into a non-singular director configuration [45]. The nematic cells with the semi-integer topological strengths $q = 1/2$ and $q = 3/2$ fabricated in the work [74] should not involve the escape into the third dimension. Indeed, the polarization-optical microscopy textures of these cells (see Ref. [74]) do not show any evidence for a radial dependence of the optical phase retardation. However, Fig. 1a and Fig. 1b demonstrate that the polarization textures might not be illustrative enough to detect the escape of the director into the third dimension, while the maps of the optical phase retardation (see Fig. 3b, d) do visualize that $\Delta\Gamma$ drops along the radial coordinate towards the centre of the structure.

To stabilize the circularly cylindrical structure against the escape into the third dimension, one could try to use nematics with negative dielectric anisotropies $\Delta\varepsilon < 0$ when applying the electric field along the cell normal. However, then the disclination line with the strength $q = +1$ might split into two disclinations with the strengths $q = +1/2$ each [75]. Theoretical considerations show that the elastic energy of the director distortions around the disclination cores of two $q = +1/2$ disclinations is twice higher if compared with a single $q = +1$ disclination [72, 73].

3.2.2. The CH-cell. In the escaped director configuration of the circular $q = +1$ disclination, the director tends to be vertical and oriented along the axis of the structure deeply in the bulk. Then a non-singular director configuration is expected in the bulk, if one of the substrates of the CC-cell is replaced by a substrate providing the homeotropic director alignment. The cell assembled of the circularly rubbed and homeotropic substrates is nothing but the CH-cell. The disclination in the CH-cell is expected to be reduced to a point defect, a 'boojume' located at the centre of the circular rubbing on the substrate, and no defect is expected in the bulk and at the homeotropic substrate.

Another feature of the homeotropic substrate is that the in-plane component of the easy axis is zero at the surface. This implies that the homeotropic anchoring is degenerate azimuthally. This feature seems to be attractive in relation to the experiment [41]. One of the substrates in this experiment is circularly rubbed and the second substrate is left un-rubbed to get an azimuthally degenerate alignment. Instead, this can in fact produce a random planar alignment rather than a degenerate one. Yet another advantage of the CH-cell in comparison with the CC-cell is that the homeotropic substrate does not require any effort to adjust it with respect to the circularly rubbed substrate. This might be compared to the CC-cell where the centres of the circular rubbings on both substrates must coincide with each other at the cell normal.

The last but not least motivation for studying the CH-cells is that the theory suggests that the elastic energy of a defect is proportional to the square of its topological strength. As a result, the point defect with the unit topological strength might be unstable against the splitting into two defects of semi-integer strengths. The structure of the light beam passing through such a defect configuration (either split or not) seems to be interesting from both fundamental and applied viewpoints.

The maps of the azimuthal orientation of the optical phase difference for the CH-cell presented in Fig. 4a, b reveal that the director distribution in this cell is not circularly symmetric. On the one hand, Fig. 3a indicates that the azimuth of polarization ellipse of the light emergent

from the cell rotates by 360° around the centre of the structure (see the data plotted in Fig. 4c). This suggests that the total topological strength of the defective structure is equal to $q = +1$ (in agreement with the symmetry of the circular rubbing), although the $\theta(\varphi)$ dependence is nonlinear and deviates significantly from the linear dependence in the first quadrant. On the other hand, the two maps of the polarization-ellipse azimuth (see Fig. 4a) and the optical phase retardation are essentially non-circular. A blue colour in Fig. 4b and Fig. 4d corresponds to the region where the director is almost vertical with respect to the substrate through the entire cell thickness, while green, yellow and red colours correspond to the places where the director tends to a planar orientation. The centre of the circular rubbing of the substrate is located between the regions of low (blue) and relatively high (green, yellow and red) phase retardations. Such a configuration of the phase retardation map would mean that the circular symmetry of the director field is evidently broken in the bulk of the cell or on the homeotropic substrate. A green colour in Fig. 4b indicates that the director tends to follow a planar (horizontal) circular alignment in the third quadrant, while a blue colour shows that the director tends to become vertical in the first quadrant. A continuous transition between the two (circularly horizontal and vertical) director orientations along the line drawn from the third quadrant to the first quadrant should involve a twist of the director. Therefore, the $\Delta\Gamma$ map shows unambiguously that the singular ($q = +1$) wedge director configuration involving a bend deformation, which is required by the circular surface alignment at one of the substrates, is replaced by the director configuration that involves a twist director deformation.

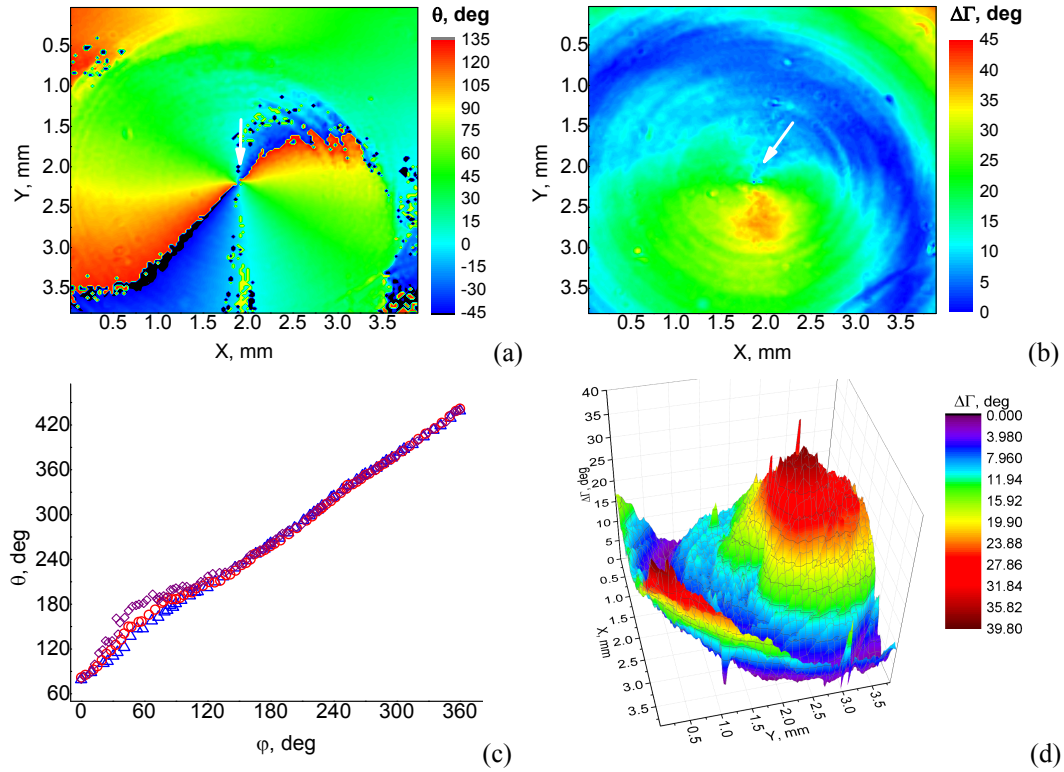

Fig. 4. Maps of orientation of the emergent light-polarization ellipse (a) and optical phase difference (b), azimuth of light-polarization ellipse as a function of azimuthal angular coordinate (c) at ρ = 0.46 mm (open triangles), 0.81 mm (open circles) and 1.22 mm (open diamonds), and 3D plot of the optical phase difference in the *XY* plane (d), as measured for the CH-cell. The centre of circular rubbing is indicated by a white arrow.

At least two scenarios can be suggested to explain why the circular symmetry is broken. First, the point defect with the strength $q = +1$ could split into the two half-integer defects, which might be too close to be resolved with the optical microscopy. Second, the structure of the director field might be of the type reported in Ref. [70], where the sectors with essentially different director distributions are inserted, thus transforming the structure into a defect with a non-trivial topological charge. Note that there is a difference between the geometry of the surface anchoring reported in Ref. [70] and that taking place in the present experiment. In Ref. [70], it is a radially hybrid director distribution which is broken by the inserted sectors, while in the CH-cell it is a circularly hybrid director configuration which could be broken by the inserted sector. Further theoretical and experimental work is needed to interpret the configuration of the director field occurring in our CH-cell. The structure of the light beams emerging from the CC- and CH-cells, which will be visualized through the interference with the reference beams of spherical and plane-wavefronts in Subsection 3.2.3, can shed additional light on the structure of defects in the above cells.

3.2.3. Visualization of optical singularities. Fig. 5 displays the interference patterns observed for the CC- (see Fig. 4a, b) and CH- (see Fig. 4c, d) cells, which have been obtained for the reference Gaussian beams of spherical (Fig. 5a,c) and plane wavefronts (Fig. 5b, d). They reveal that the object beams passing through the defective structures under test are indeed singular. The interference patterns for the CC-cell are similar to the classical patterns reported earlier for the circular disclination with $q = +1$ [41]. As seen from Fig. 5a, the interference pattern contains two well-resolved spirals. The very double-spiral interference pattern indicates that the nematic disclination has the total topological strength $|q| = 1$.

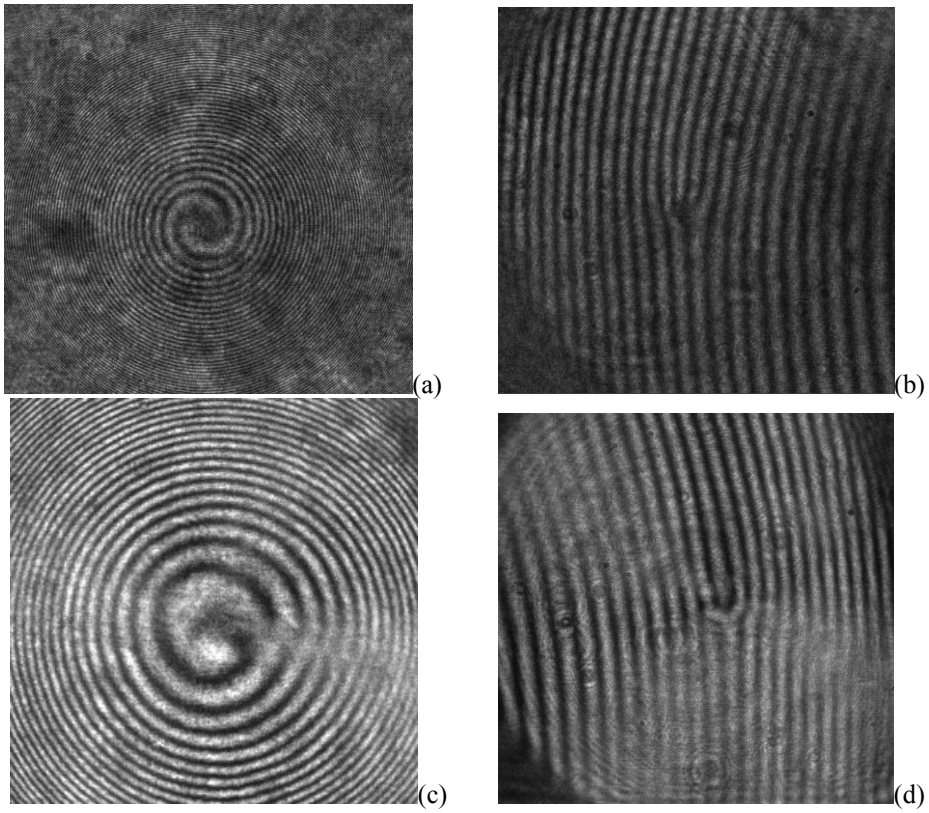

Fig. 5. Interference patterns of the vortex beam with the Gaussian beams with spherical (panels a and c) and almost plane (panels b and d) wavefronts, as observed for the CC- (a, b) and CH- (c, d) cells.

When the same singular object beam interferes with the reference beam with the plane wavefront, the interference pattern contains a fork-like feature, with two bright extra fringes inserted into a system of bright parallel (equidistant) fringes (see Fig. 5b). This pattern reminds a dislocation of the Burgers vector equal to the doubled spatial period in a system of smectic LC layers [73]. Again, the two additional bright fringes inserted into the system of bright parallel fringes suggest that a dislocation-like interference pattern is formed due to the disclination with the total topological strength $|q|=1$. This agrees well with the circular geometry of the planar surface anchoring occurring at the bounding cell substrates.

Although the symmetry of the surface anchoring occurring at one of the bounding substrates of the CH-cell is also circular, the corresponding interference patterns are essentially different from those observed for the CC-cell. The pattern obtained for the reference beam with the spherical wavefront (see Fig. 5c) has a definitely non-circular symmetry. It seems to be formed by a superposition of spirals of the opposite (left and right) handednesses. The latter suggests that the chiral symmetry of the CH-structure is broken into two twisted domains of the opposite handednesses. A coexistence of the two alternative twists can be associated with achiral symmetry of the nematic molecules. Moreover, a presence of the director twist suggests that, most probably, the disclinations have twist or mixed (twist-wedge) characters. Their character can hardly be purely wedge-like, in agreement with the conclusions drawn in Subsection 3.2.2.

It is important that the twist elastic constant K_2 for the conventional nematics with small rod-like molecules is less than the splay (K_1) and bend (K_3) elastic constants (usually, we have the inequalities $K_2 < K_1 < K_3$). Then the twist disclination should have a lower elastic energy than that of the disclination with a wedge character. Topologically there is no difference between the twist and wedge disclinations of the same strength; they can be continuously transformed into each other. However, their elastic energies are different. An integer-strength twist disclination is non-singular, and a semi-integer-strength disclination is singular, in compliance with their wedge-like counterparts. In addition, the core of a semi-integer-strength twist disclination is usually thinner than that of a semi-integer-strength wedge disclination [72]. The pure bulk elastic energy of an integer-strength disclination is twice higher than that of the sum of two semi-integer-strength disclinations. Since the total bulk energy of the two disclinations with $|q|=1/2$ is lower than that of the $|q|=1$ disclination and the elastic energy of a twist disclination is usually lower than that of a wedge disclination, one could expect at first glance that the $|q|=1$ disclinations should always split into two twist disclinations with $|q|=1/2$. However, the $|q|=1$ disclinations in real nematic samples are not less frequent than the disclinations with $|q|=1/2$. The explanation is that the integer- and semi-integer-strength wedge and twist disclinations have different surface elastic energy costs.

Note also that the CC- and CH-cells differ by the anchoring at one of their substrates. The anchoring strength at the homeotropic substrate is several orders of magnitude lower than that at the planar rubbed substrate [Compare the typical zenithal-anchoring strength coefficients 10^{-3} J/m^2 for a rubbed polymer-covered substrate to the values 10^{-6} J/m^2 peculiar for a substrate with the homeotropic anchoring.] It is likely that the splitting of the $q=+1$ disclination into two $q=+1/2$ disclinations in the CC-cell is hindered by a strong surface anchoring at the

rubbed polymer-covered substrates and, in addition, the stability of the $q=+1$ disclination is favoured by the escape of the director into the third dimension.

Therefore, it is quite plausible that the circular integer-strength wedge disclination in the CH-cells might transform into the twist disclination with a non-trivial topological charge, in a fashion roughly similar to that described in Ref. [70]. The difference is that in Refs. [70, 71] the sectors with an extraordinaire director distribution are inserted into the radial configuration of the director, while in our case the extraordinaire sectors are inserted into the circular distribution.

For the plane-wavefront reference beam, the interference pattern contains two fork-like features oriented in the opposite (upward and downward) directions. The upward-oriented dislocation fork is formed by a bright fringe, which splits into two fringes, and one fringe inserted in between. Then one bright fringe which forms the handle of the dislocation fork splits into three bright fringes, thus forming its tines. Two extra bright fringes suggest that the dislocation fork is formed by the light beam passing through a nematic disclination with the strength $|q|=1$. The second dislocation fork observed in the pattern is oriented downward. It is formed by two bright fringes with one extra fringe inserted in between. Such a dislocation fork could be formed by the object beam passing through the nematic disclination with the topological strength $|q|=1/2$. In agreement with the conclusion given above for the pattern detected in the case of spherical-wavefront reference beam, the pattern shown in Fig. 5d could be obtained if the $q=+1$ disclination splits into two disclinations with $q=+1/2$. The opposite (upward and downward) orientations of the fork-like features implies that the two $q=+1/2$ disclinations have the twist character and the opposite handednesses. Splitting of the integer-strength defect into a pair of semi-integer defects could also be accompanied by insertion of additional sectors in the way similar to that reported in Refs. [70, 71].

One way or another, the interference patterns shown in Fig. 5c, d confirm that the circular symmetry of the director distribution imposed by the circular rubbing is broken. The exact director configuration resulted from this symmetry breaking still has to be investigated. Note also that the optical properties of the CH-cells might be complicated by the phenomena of optical spatial dispersion due to essentially non-uniform director distributions through the cell thickness.

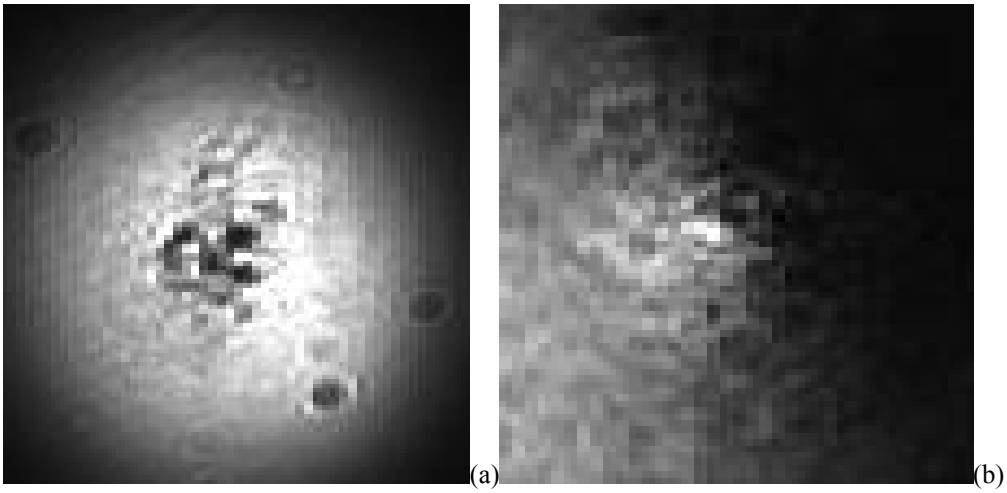
(a) (b)

Fig. 6. Vortex doughnut modes detected for the CC- (a) and CH- (b) cells.

The doughnut mode obtained for the CC-cell is shown in Fig. 6a. Although here the central part of the pattern is somewhat imperfect around its centre, it is still dark in the very centre. This agrees with a classical pattern of the vortex mode [76]. The dark central part observed for the CH-cell is accompanied by even higher imperfections around it. This should be addressed to the fact that the circular symmetry of the director distribution is essentially broken. Gradual vanishing of the intensity towards the right part of the pattern is associated with the distribution of the optical phase difference shown in Fig. 6b, where it drops to zero in the right-hand part of the $\Delta\Gamma$ map.

4. Concluding remarks

Among the variety of optical elements used for generating vector optical vortices, the LC cells containing topological defects are of particular importance. Because of simplicity of their preparation, they represent one of the most popular techniques. It is very attractive that a topological defect in a nematic cells can be induced by a specially designed pattern of the easy axis along which the nematic director is oriented at the surface. It is believed that, due to orientation elasticity of nematics, the director distribution imposed by the surface anchoring can successfully propagate throughout the bulk. It is indeed so in many cases, though not always. If one forms a distribution of the easy axis that induces the defect of the half-integer strength on both substrates such that the singular points on the opposite substrates lie on a cell normal, then the director distribution indeed is reproduced inside the overall bulk. As a result, the disclination line with the singular core connects the surface director singularities through the cell thickness.

For a cell assembled of two circularly rubbed and coaxially superimposed substrates, one expects formation of the defects with the topological strength $q = +1$ on the surfaces. However, this time the singular director distribution does not propagate through the bulk. The disclinations of the half-integer and integer topological strengths in uniaxial nematics belong to different topological classes. Namely, the half-integer-strength disclinations represent true defects in the sense that their cores cannot be transformed into a non-singular configuration by any continuous transformation, i.e. their cores are always singular. On the contrary, the integer-strength disclinations are topologically equivalent to a non-singular state. The mechanism that transforms the core of the integer-strength disclination into a non-singular configuration is termed as the escape of the director into the third dimension. The director in the escaped configuration is parallel to the disclination line, thus making it non-singular. For the director circularly aligned on the bounding surfaces, the wedge disclination transforms into the twist disclination. Then the resulting director configuration is not singular in the bulk.

In this paper we have presented the experimental results related to optical characterization of the cells with circularly planar and circularly hybrid surface alignment, using the imaging polarimetry. Our experiments reveal that the director field in the cells is more complicated than can be expected from the geometry of the imposed surface anchoring. Namely, the director field in the cell with two circularly rubbed substrates (i.e., the CC-cell) indeed manifests the escape into the third dimension. The experiment demonstrates that the excessive optical phase retardation $\Delta\Gamma$ decreases radially towards the centre of the structure. Such a coordinate behaviour of $\Delta\Gamma$ agrees with the configuration of the director escaped into the third dimension through the twist deformation. However, one should take into account that the director escape is hindered near the substrates under the condition of a strong zenithal surface anchoring. As a result, the involved director deformation is not a pure twist but involves also bend and splay deformations. We have offered a model that describes the escaped director distribution inside the CC-cell with an infinitely large zenithal surface anchoring.

The interference of the reference Gaussian beams having the spherical and plane wavefronts with the object beam passed through the CC-cells has confirmed that the latter beam is optically singular. The two spirals of the same handedness, which are akin to the Fermat's double spiral, have been obtained for the spherical reference beam. Then the fork-like dislocation pattern with two extra fringes inserted into the system of parallel fringes visualizes the fact that the optical singularity is associated with the orbital angular momentum $l = 2$, which is induced by the nematic defect of the topological strength $q = +1$. Importantly, the escape of the director into the third dimension inside the CC-cell does not affect the topology of the optical vector singularity defect. Although the core of the $q = +1$ disclination becomes non-singular due to the escape into the third dimension, it remains singular in the centres of circular rubbing on the substrates due to a strong zenithal surface anchoring. In the escaped configuration, the azimuth of light polarization is undefined along the disclination axis where the director is parallel to the disclination. In other words, it can acquire arbitrary values. As a result, the vector optical singularity formed in the centre of the rubbed entrance substrate surface propagates with no modification throughout the cell thickness, since the light always propagates along the optic axis along the disclination. At the exit substrate, the singular beam meets another 0D defect which is topologically identical to that occurring at the entrance surface. Therefore the emergent light beam remains singular and has the orbital angular momentum $l = 2$.

Replacement of one of the circularly rubbed substrates by the substrate with the homeotropic anchoring, which occurs in the CH-cell, provides several advantages if compared with the case of the CC-cell. First, it facilitates easier cell preparation because there is no need to adjust the positions of the easy-axis patterns on the bounding substrates. Second, the homeotropic anchoring is azimuthally degenerate and so free of random director distortions in the azimuthal plane. Third, the geometry of the CH-cell allows one to reduce a linear (1D) disclination with $q = +1$ to a point (i.e., 0D) defect or defects at the surface with the circular rubbing. The theoretical estimations show that the elastic energy of the line disclination connecting the two substrate is lower for the $q = +1$ disclination with its core escaped into the third dimension, in comparison with the total energy of the two $q = +1/2$ disclination with singular cores. For this reason, the $q = +1$ disclination in the CC-cells is favoured against its splitting into the two half-integer disclinations.

The situation in the CH-cells is different. Here the disclination line reduces to the point defect at the substrate with the circular rubbing. The theory suggests that the bulk elastic energy of the point defect with $q = +1$ is higher than the energy of the two point defects with $q = +1/2$. Therefore the splitting of a unit integer-strength defect into two half-integer defects can be expected. The imaging polarimetry has indeed demonstrated that the map of the excessive optical retardation is not circularly symmetric as it must have been for the point defect with $q = +1$. An essentially broken circular symmetry of the $\Delta\Gamma$ map points toward a splitting into two half-integer defects. The interferometry of the object light beam passed through the CH-cell with the reference beams of the spherical and plane wavefronts testifies that the interference patterns are unambiguously different from those expected for a single unit-integer-strength defect. The interference patterns obtained with both the spherical and plane wavefronts indicate the existence of two defects. The polarization microscopy alone does not provide evidence enough for the defect splitting, which can be explained by the fact that this splitting occurs on the scales below the microscope resolution. Nonetheless, the imaging polarimetric data combined with the interference results support the splitting scenario.

Additional experiments are needed in order to interpret the exact director configuration inside the CH-cell. It is also important to check whether the escape into the third dimension would take place in much thinner LC cells, especially in the cells with the thicknesses of about 6 μm, which provide the optical phase retardation equal to the half of the (red laser) light wavelength. Note that application of an external electric field to the CC- and CH-cells filled with nematics of positive and negative dielectric anisotropies might be helpful for reconstructing the director field. Moreover, this might also elucidate new interesting features of the structure of the singular beams. Optical characterization at the green-light wavelengths, where dye-doped nematics strongly absorb the light, would also be of great interest. These and some other experiments are now in progress.

References

1. Schatz M F and Neitzel G P, 2001. Experiments on thermocapillary instabilities. Ann. Rev. Fluid Mech. **33**: 93–127.
2. Forbes A, 2019. Common elements for uncommon light: vector beams with GRIN lenses. Light Sci. Appl. **8**: 111.
3. Rongxuan Wang, Law A C, Garcia D, Shuo Yang and Zhenyu James Kong, 2021. Development of structured light 3D-scanner with high spatial resolution and its applications for additive manufacturing quality assurance. Int. J. Adv. Manuf. Technol. **117**: 845–862.
4. Wuchen Zhang, Deborah A Kosiorek and Amy N Brodeur, 2020. Application of structured-light 3-D scanning to the documentation of plastic fingerprint impressions: A quality comparison with traditional photography. J. Forensic Sci. **65**: 784–790.
5. Allen L, Beijersbergen M W, Spreeuw R J C and Woerdman J P, 1992. Orbital angular momentum of light and the transformation of Laguerre–Gaussian laser modes. Phys. Rev. A. **45**: 8185–8189.
6. Qiwen Zhan, 2009. Cylindrical vector beams: from mathematical concepts to applications. Adv. Opt. Photon. **1**: 1–57.
7. Mair A, Vaziri A, Weihs G and Zeilinger A, 2001. Entanglement of the orbital angular momentum states of photons. Nature. **412**: 313–316.
8. Leach J, Jack B, Romero J, Jha A K, Yao A M, Franke-Arnold S, Ireland D G, Boyd R W, Barnett S M and Padgett M J, 2010. Quantum correlations in optical angle-orbital angular momentum variables. Science. **329**: 662–665.
9. Quabis S, Dorn R, Eberler M, Glockl O and Leuchs G, 2000. Focusing light to a tighter spot. Opt. Commun. **179**: 1–7.
10. Youngworth K S and Brown T G, 2000. Focusing of high numerical aperture cylindrical-vector beams. Opt. Express **7**: 77–87.
11. Grier D G, 2003. A revolution in optical manipulation. Nature. **424**: 810–816.
12. Mawet D, Riaud P, Absil O and Surdej J, 2005. Annular groove phase mask coronagraph. Astro. Phys. **633**: 1191–1200.
13. Liu Y, Cline D and He P, 1999. Vacuum laser acceleration using a radially polarized CO_2 laser beam. Nucl. Instrum. Meth. Phys Res. A. **424**: 296–303.
14. Kimura W D, Kim G H, Romea R D, Steinhauer L C, Pogorelsky I V, Kusche K P, Fernow R C, Wang X and Liu Y, 1995. Laser acceleration of relativistic electrons using the inverse Cherenkov effect. Phys. Rev. Lett. **74**: 546–549.
15. Basistiy V I, Soskin M S and Vasnetsov M V, 1995. Optical wavefront dislocations and their properties. Opt. Commun. **119**: 604–612.

16. Long Zhu and Jian Wang, 2014. Arbitrary manipulation of spatial amplitude and phase using phase-only spatial light modulators. Sci. Rep. **4**: 7441.
17. Long Zhu and Jian Wang, 2019. A review of multiple optical vortices generation: methods and applications. Front. Optoelectron. **12**: 52–68.
18. Beijersbergen M W, Coerwinkel R P C, Kristensen M and Woerdman J P, 1994. Helical-wavefront laser beams produced with a spiral phaseplate. Opt. Commun. **112**: 321–327.
19. Stalder M and Schadt M, 1996. Linearly polarized light with axial symmetry generated by liquid-crystal polarization converters. Opt. Lett. **21**: 1948–1950.
20. Zhi-Xiang Li, Ya-Ping Ruan, Peng Chen, Jie Tang, Wei Hu, Ke-Yu Xia and Yan-Qing Lu, 2021. Liquid crystal devices for vector vortex beams manipulation and quantum information applications [Invited]. Chin. Opt. Lett. **19**: 112601.
21. Skab I, Vasylkiv Y, Savaryn V and Vlokh R, 2011. Optical anisotropy induced by torsion stresses in $LiNbO_3$ crystals: appearance of an optical vortex. J. Opt. Soc. Amer. A. **28**: 633–640.
22. Skab I, Vasylkiv Yu, Smaga I and Vlokh R, 2011. Spin-to-orbital momentum conversion via electro-optic Pockels effect in crystals. Phys. Rev. A. **84**: 043815.
23. Skab I, Vasylkiv Yu, Vlokh R, 2012. Induction of optical vortex in the crystals subjected to bending stresses. Appl. Opt. **51**: 5797–5805 .
24. Niv A, Biener G, Kleiner V and Hasman E, 2004. Propagation-invariant vectorial Bessel beams obtained by use of quantized Pancharatnam-Berry phase optical elements. Opt. Lett. **29**: 238–240.
25. Niv A, Biener G, Kleiner V and Hasman E, 2005. Rotating vectorial vortices produced by space-variant subwavelength gratings. Opt. Lett. **30**: 2933–2935.
26. Niv A, Biener G, Kleiner V, Hasman E, 2006. Manipulation of the Pancharatnam phase in vectorial vortices. Opt. Express. **14**: 4208–4220.
27. Oron R, Blit S, Davidson N, Friesem A A, Bomzon Z and Hasman E, 2000. The formation of laser beams with pure azimuthal or radial polarization. Appl. Phys. Lett. **77**: 3322–3324.
28. Toussaint K C Jr, Park S, Jureller J E and Scherer N F, 2005. Generation of optical vector beams with a diffractive optical element interferometer. Opt. Lett. **30**: 2846–2848.
29. Yao-Wei Huang, Rubin N A, Ambrosio A, Zhujun Shi, Devlin R C, Cheng-Wei Qiu and Capasso F, 2019. Versatile total angular momentum generation using cascaded J-plates. Opt. Express. **27**: 7469–7484.
30. Rubano A, Cardano F, Piccirillo B and Marrucci L, 2019. Q-plate technology: a progress review [Invited]. J. Opt. Soc. Amer. B. **36**: D70–D87.
31. Piccirillo B, D'Ambrosio V, Slussarenko S, Marrucci L and Santamato E, 2010. Photon spin-to-orbital angular momentum conversion via an electrically tunable q-plate. Appl. Phys. Lett. **97**: 241104.
32. Slussarenko S, Piccirillo B, Chigrinov V, Marrucci L and Santamato E, 2013. Liquid crystal spatial-mode converters for the orbital angular momentum of light. J. Opt. **15**: 025406.
33. Nastishin Yu A, Dudok T, Savaryn V, Kostyrko M, Vasylkiv Yu, Hrabchak V, Ryzhov Ye and Vlokh R, 2021. Liquid crystal textures and optical characterization of a dye-doped nematic for generating vector beams. Ukr. J. Phys. Opt. **22**: 151–164.
34. Etienne Brasselet, Naoki Murazawa, Hiroaki Misawa and Saulius Juodkazis, 2009. Optical vortices from liquid crystal droplets. Phys. Rev. Lett. **103**: 103903.
35. Loussert C, Delabre U and Brasselet E, 2013. Manipulating the orbital angular momentum of light at the micron scale with nematic disclinations in a liquid crystal film. Phys. Rev. Lett. **111**: 037802.

36. Frank F C, 1958. I. Liquid crystals. On the theory of liquid crystals. Disc. Farad. Soc. **25**: 19–28.
37. Moreno I, Sanchez-Lopez M M, Badham K, Davis J A and Cottrell D M, 2016. Generation of integer and fractional vector beams with q-plates encoded onto a spatial light modulator. Opt. Lett. **41**:1305–1308.
38. Barboza R, Bortolozzo U, Assanto G, Vidal-Henriquez E, Clerc M G and Residori S, 2013. Harnessing optical vortex lattices in nematic liquid crystals. Phys. Rev. Lett. **111**: 093902.
39. Wei Ji, Chun-Hong Lee, Peng Chen, Wei Hu, Yang Ming, Lijian Zhang, Tsung-Hsien Lin, Vladimir Chigrinov and Yan-Qing Lu, 2016. Meta-q-plate for complex beam shaping. Sci. Rep. **6**: 25528.
40. Yao-Han Huang, Ming-Shian Li, Shih-Wei Ko and Andy Y-G Fuh, 2013. Helical wavefront and beam shape modulated by advanced liquid crystal q-plate fabricated via photoalignment and analysed by Michelson's interference. Appl. Opt. **52**: 6557–6561.
41. Marrucci L, Manzo C and Paparo D, 2006. Pancharatnam–Berry phase optical elements for wavefront shaping in the visible domain: switchable helical modes generation. Appl. Phys. Lett. **88**: 221102.
42. Clark N L, 1985. Surface memory effects in liquid crystals: Influence of surface composition. Phys. Rev. Lett. **55**: 292–295.
43. Glushchenko A, Kresse H, Reshetnyak V, Reznikov Yu and Yaroshchuk O, 1997. Memory effect in filled nematic liquid crystals. Liq. Cryst. **23**: 241– 246.
44. Nych A B, Reznikov D Yu, Boiko O P, Nazarenko V G, Pergamenshchik V M and Bos P, 2008. Alignment memory of a nematic liquid crystal and thermal isotropization of the surface adsorbed layer. Europhys. Lett. **81**: 16001.
45. Cladis P E and Kleman M, 1972. Non-singular disclinations of strength S = +1 in nematics. J. Physique. **33**: 591–598.
46. Meyer R, 1973. On the existence of even indexed disclinations in nematic liquid crystals. Phil. Mag. **27**: 405–424.
47. Melzer D and Nabarro F R N, 1977. Optical studies of a nematic liquid crystal with circumferential surface orientation in a capillary. Phil. Mag. **35**: 901–906.
48. Marrucci L, 2008. Generation of helical modes of light by spin-to-orbital angular momentum conversion in inhomogeneous liquid crystals. Mol. Cryst. Liq. Cryst. **488**: 148–162.
49. Nastishin Yu A and Dudok T H, 2013. Optically pumped mirrorless lasing. A review. Part I. Random lasing. Ukr. J. Phys. Opt. **14**: 146–170.
50. Dudok T H and Nastishin Yu, 2014. Optically pumped mirrorless lasing. A Review. Part II. Lasing in photonic crystals and microcavities. Ukr. J. Phys. Opt. **15**: 47–67.
51. Dudok T H, Krupych O M, Savaryn V I, Cherpak V V, Fechan A V, Gudeika D, Grazulevicius J V, Pansu B and Nastishin Yu A, 2014. Lasing in a cholesteric liquid crystal doped with derivative of triphenylamine and 1,8-naphthalimide, and optical characterization of the materials. Ukr. J. Phys. Opt. **15**: 162–172.
52. Dudok T H, Savaryn V I, Fechan AV, Cherpak V V, Pansu B and Nastishin Yu A, 2014. Dot lasers: isotropic droplets in a cholesteric matrix, and vice versa. Ukr. J. Phys. Opt. **15**: 227–232.
53. Dudok T H, Savaryn V I, Krupych O M, Fechan A V, Lychkovskyy E, Cherpak V V, Pansu B and Nastishin Yu A, 2015. Lasing in imperfectly aligned cholesterics. Appl. Opt. **54**: 9644–9653.
54. Dudok T H, Savaryn V I, Meyer C, Cherpak V V, Fechan A V, Lychkovskyy E I, Pansu B and Nastishin Yu A, 2016. Lasing cholesteric capsules. Ukr. J. Phys. Opt. **17**: 169–175.
55. Chapran M, Angioni E, Findlay N J, Breig B, Cherpak V, Stakhira P, Tuttle T, Volyniuk D,

Grazulevicius J V, Nastishin Yu A, Lavrentovich O D and Skabara P J, 2017. An ambipolar BODIPY derivative for a white exciplex OLED and cholesteric liquid crystal laser towards multi-functional devices. Appl. Mater. & Interfaces. **9**: 4750−4757.

56. Konstantinova A F, Grechushnikov B N, Bokut B V and Valyashko Ye G. Optical Properties of Crystals. Minsk: Navuka i Teknnika, 1995.
57. Nastishin Yu A and Nastyshyn S Yu, 2011. Explicit representation of extended Jones matrix for oblique light propagation through a crystalline slab. Ukr. J. Phys. Opt. **12**: 191–201.
58. Nastishin Yu A and Nastyshyn S Yu, 2013. Differential and integral extended Jones matrices for oblique light propagation through a deformed crystal. Phys. Rev. A. **87**: 033810.
59. Nastyshyn S Yu, Bolesta I M, Tsybulia S A, Lychkovskyy E, Yakovlev M Yu, Ryzhov Ye, Vankevych P I and Nastishin Yu A, 2018. Differential and integral Jones matrices for a cholesteric. Phys. Rev. A. **97**: 053804.
60. Nastyshyn S Yu, Bolesta I M, Tsybulia S A, Lychkovskyy E, Fedorovych Z Ya, Khaustov D Ye, Ryzhov Ye, Vankevych P I and Nastishin Yu A, 2019. Optical spatial dispersion in terms of Jones calculus. Phys. Rev. A. **100**: 013806.
61. Mauguin C, 1911. Sur les cristaux liquides de Lehman. Bull. Soc. Fr. Miner. Cristallogr. **34**: 71–117.
62. Guang-Hoon Kim, Hae June Lee, Jong-Uk Kim and Hyyong Suk, 2003. Propagation dynamics of optical vortices with anisotropic phase profiles. J. Opt. Soc. Amer. B. **20**: 351–359.
63. Kleman M. Points, lines and walls. In: Liquid crystals, magnetic systems and various ordered media. Chichester: Wiley, 1983.
64. Nabarro F R N, 1972. Singular lines and singular points of ferromagnetic spin systems and of nematic liquid crystals. J. Physique. **33**: 1089–1098.
65. Nastishin Yu A, Polak R D, Shiyanovskii S V, Bodnar V H and Lavrentovich O D, 1999. Nematic polar anchoring strength measured by electric field techniques. J. Appl. Phys. **86**: 4199–4213.
66. Nastishin Yu A, Polak R D, Shiyanovskii S V and Lavrentovich O D, 1999. Determination of nematic polar anchoring from retardation versus voltage measurements. Appl. Phys. Lett. **75**: 202–204.
67. Shenoy D, Gruenberg K, Naciri J, Shashidhar R, Nastishin Yu, Polak R and Lavrentovich O D, 1999. Device properties and polar anchoring of nematic molecules at photodimerized surfaces. Proc. SPIE. **3635**: 24–30.
68. Nantomah K, 2018. On some properties and inequalities of the sigmoid function. RGMIA Res. Rep. Coll. **21**: 89.
69. Khaustov D Ye, Nastishin Yu A and Khaustov Ya Ye, 2021. Probability of the visual search task execution as a sigmoid function. Weap. Milit. Equip. **3**: 80–94.
70. Lavrentovich O D and Nastishin Yu A, 1987. Defects with nontrivial topological charges in hybrid-aligned films of nematic liquid crystal. Sov. Phys. Cryst. **34**: 914–917
71. Lavrentovich O D and Nastishin Yu A, 1990. Defects in degenerate hybrid aligned nematic liquid crystals. Europhys. Lett. **13**: 135–141.
72. Kleman M and Laverntovich O D. Soft Matter Physics: an Introduction. New York: Springer-Verlag, 2003.
73. Kleman M, Lavrentovich O D and Nastishin Yu A. Dislocation and disclination in mesomorphic phases. Vol. 12, pp. 147–271. In: Dislocations in Solids. Ed by Nabarro F R N and Hirth J P, Elsevier, 2004.

74. Slussarenko S, Murauski A, Chigrinov V, Tao Du, Marrucci L and Santamato E, 2011. Tunable liquid crystal q-plates with arbitrary topological charge. Opt. Express. **19**: 4085–4090.
75. Susser A L, Harkai S, Kralj S and Rosenblatt C, 2020. Transition from escaped to decomposed nematic defects, and vice versa. Soft Matter. **16**: 4814–4822,
76. White A G, Smith C P, Heckenberg N R, Rubinsztein-Dunlop H, McDuff R, Weiss C O and Tamm C, 1991. Interferometric measurements of phase singularities in the output of a visible laser. J. Mod. Opt. **38**: 2531–2541.

Dudok T., Skab I., Mys O., Krupych O., Nastishin Yu. A., Kurochkin O., Nazarenko V., Ryzhov Ye., Chernenko A. D. and Vlokh R. 2023. Optical vector vortices generated with circularly planar and circularly hybrid nematic cells. Ukr.J.Phys.Opt. **24**: 22 – 45. doi: 10.3116/16091833/24/1/22/2023

Анотація. *Серед різноманіття оптичних елементів, які використовують для генерування векторних і вихрових світлових пучків, на окрему увагу заслуговують рідкокристалічні комірки, що містять топологічні дефекти. На сьогодні вони є однією з найпопулярніших методик через простоту їхнього приготування. У цій роботі досліджено оптичні сингулярності для лазерних променів, які проходять крізь комірку з круглим планарним розташуванням директора на обох підкладках (т.зв. CC-комірку). Інший об'єкт наших досліджень – це т.зв. CH-комірка з циркулярним планарним упорядкуванням на одній підкладці та гомеотропним (тобто перпендикулярним до площини підкладки) упорядкуванням на протилежній підкладці. Виконано оптичну характеризацію CC- і CH-комірок за допомогою поляризаційної оптичної мікроскопії та поляриметрії формування зображень. Оптичні особливості об'єктних пучків, що проходять крізь згадані комірки, візуалізовано за допомогою їхньої інтерференції з квазісферичними та квазіплоскохвильовими опорними ґаусовими пучками. Для CC-комірок очікується утворення на поверхнях дефектів із топологічною силою q=+1. Сингулярний розподіл директора не поширюється крізь об'єм комірки через ефект втечі в третій вимір. Аналізуючи літературу про застосування рідкокристалічних дисклінацій для генерування сингулярних пучків, ми виявили, що втечу директора в третій вимір зазвичай ігнорують для дисклінацій цілочисельної сили. Крім того, ми докладно проаналізували, як втеча в третій вимір виявляється при поширенні світла крізь CC-комірки. Для CH-комірок виявлено, що оптичні картини, одержані за допомогою поляризаційної оптичної мікроскопії, поляриметрії зображення та методів інтерференції, вказують на те, що кругова симетрія структури зразка істотно порушена.*

Ключові слова: *рідкі кристали, оптичні вихори, топологічні дефекти, оптична індикатриса, оптична різниця фаз*